CHAPTER 6

RESULTS AND DISCUSSION - PART 3: PREPARATION AND CHARACTERIZATION OF PZT/CuO THIN FILMS

Ferroelectric materials with perovskite structure have been extensively studied due to their technological importance and unique electromechanical properties. Lead zirconate titanate (PZT) is a prototypical example of these materials [154]. Tailored properties of ferroelectric materials may be obtained by aliovalent dopants which substitute a part of host atoms and modify their electrical properties [155]. There are two principal categories of dopants: donor dopants or soft doping, which are higher-valence substitution; and acceptor dopants or hard doping, which are lower-valence substitutions. Compared to soft PZT, hard PZT normally has lower permittivity, smaller dielectric loss, poorer piezoelectric coefficients, but higher mechanical quality factor Q_m and higher resistance to poling by mechanical stresses [156]. Hard doped PZT are generally applied in a high power ultrasonic transducer. The high Q_m of hard PZT may also improve the fatigue properties of PZT. CuO has been used as an additive to lower the sintering temperature of various piezoelectric ceramics, resulting in hard doping effect [157]. Some studies proposed that CuO-added piezoelectric ceramics were superior in piezoelectric properties to those of undoped ceramics [158, 159]. However, the effects of CuO addition on ferroelectric properties remain largely unknown. Moreover, the fatigue property of CuO-added PZT system is an interesting topic to investigate due to its high

Q_m value as mentioned earlier. The result in this chapter will report the effect of CuO on Phase, microstructure and electrical properties of PZT films were investigated to figure out the optimized condition of this composite system for studying of ferroelectric fatigue and being compared to that of pure PZT thin films.

6.1 Phase of PZT/CuO thin films

X-ray diffraction results of PZT/*x*CuO films, where x = 0, 0.1, 0.2, 0.3, 0.4, 0.5 and 1 wt%, are shown in Fig. 6.1. The data indicated that, when the films were annealed at 600 °C, all the films possessed a crystalline perovskite structure with a second phase appearing at higher CuO added contents (≥ 0.4wt%). The second phase was matched with $Pb(Cu_2O_2)$ phase (ICSD No. 400657), which was a reaction of PbO and CuO. The orientation analysis was carried out on a basis of XRD peak intensity ratio of the PZT/CuO thin films, as shown in Fig. 6.2. The (010) orientation increased with increasing CuO concentration. In contrast, the intensity ratio of (110), (111) and (020) decreased with increasing CuO concentration. The (120) and (211) reflections did not show any change in the intensity ratio. It was believed that the growth of (010)-oriented grains was influenced by microcrystallization of the PbO(010) seed layer during pyrolysis in sol-gel PZT films [130]. Since CuO has been known as a good sintering aid for PZT, a possible formation of PbO(010) seed layer could be due to a reduction of sintering temperature by CuO addition which would also affect the film orientation. This, therefore, caused the intensity ratio of (010) orientation to increase while causing that of (110) to decrease (Fig. 6.2). Moreover, CuO seemed to partially substitute at the B-site of the PZT lattice, which could induce PbO microcrystallization as a consequence of charge neutrality. However, some PbO also reacted with the remaining CuO to form the second phase.

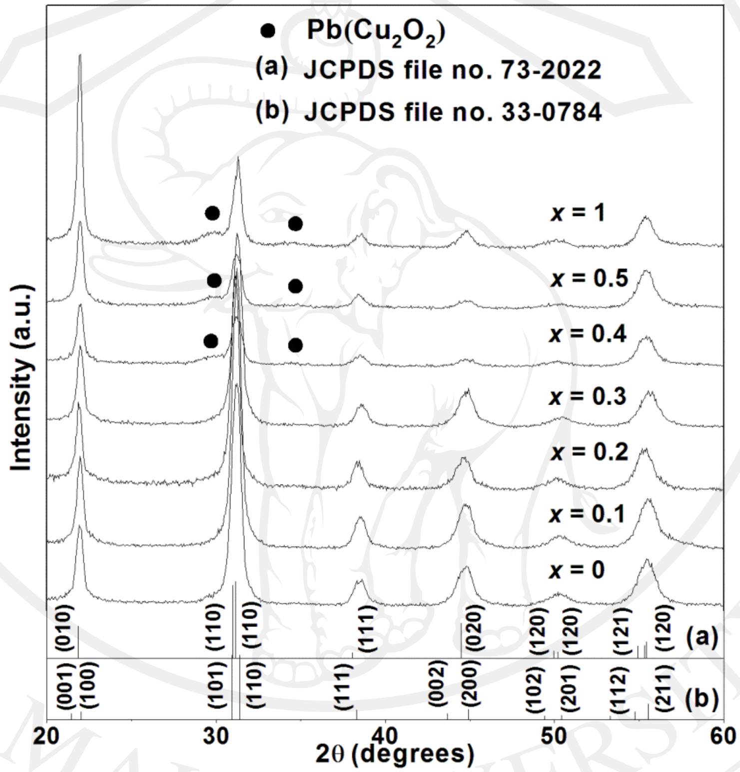

Figure 6.1 XRD patterns of PZT/*x*CuO films, where *x* = 0, 0.1, 0.2, 0.3, 0.4, 0.5 and 1 wt%. The films were pre-heated at 400°C for 30 min and annealed at 600°C for 30 min.

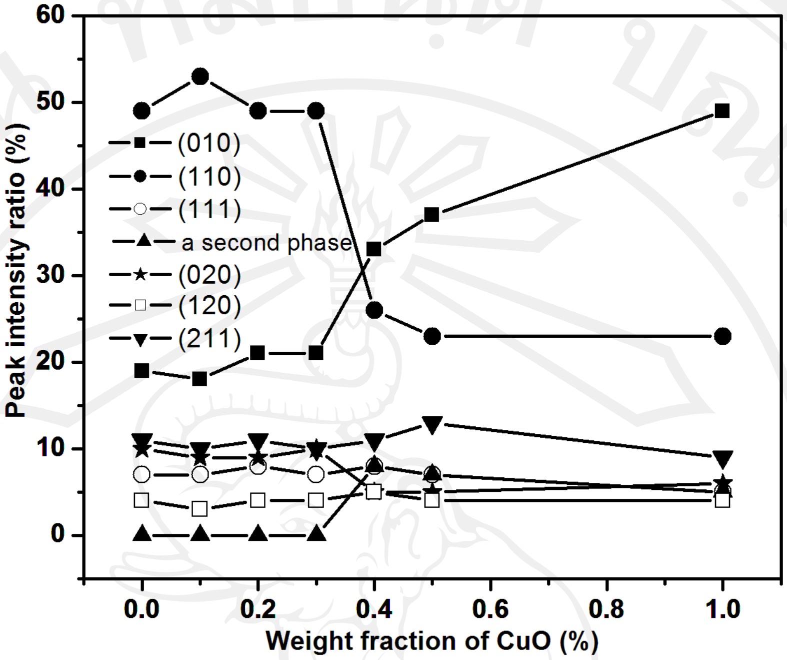

Figure 6.2 Percentages of the PZT peak intensity ratio as a function of CuO concentration. The peak intensity ratios were calculated according to (010): $I_{(010)}/[I_{(010)}+I_{(110)}+I_{(111)}+I_{(Sp)}+I_{(202)}+ I_{(120)}+I_{(211)}] \times 100$.

6.2 Microstructure of PZT/CuO thin films

SEM micrographs show microstructural evolution of PZT/CuO films (Fig. 6.3). All films were dense and crack-free although tiny cracks were present on the surfaces of the films. The tiny cracks were carbon grains deposited on the surface. Specimens need to be grounded electrically to prevent the accumulation of electrostatic charge at the surface of nonconductive specimens. Tiny cracks also existed at the cross section of the films (Fig. 6.4). However, this crack was not found in PZT/WO_3 film. It is believed to be due to the higher magnification SEM pictures by using a magnification × 30,000 for PZT/WO_3 system and × 40,000 for PZT/CuO system. Comparing the surface to the cross section of the films, different microstructures between the two were observed. The SEM micrographs also showed the hillock-like structure of nanometer-sized grains aggregated as found in PZT/WO_3 system, and it was due to the compressive stress as describe in the previous chapter. Few variations in hillock size were due to the uncontrollable preparation environment, as described in previous chapter.

Figure 6.4 shows a comparison of the ×40,000-magnified cross sections of PZT/CuO films with a ×30,000 magnified PZT film. It was found that the first layer of all films is about 350 nm thick and the second layer about 700 nm thick (Fig. 6.4). The cross sections of all films showed dense microstructure. Moreover, all films showed random orientation grains with nanometer-sized aggregated structure. The observed grain sizes are shown in Table 6.1. It indicated that the relatively low amount of CuO addition promoted the grain growth of PZT. As found in previous work, the physical properties of oxides depended strongly on the defect chemistry and the nature and concentration of foreign atoms incorporated into the crystal lattice [160]. For PZT/CuO films, the size of Cu^{2+} (0.73 Å) is approximately the same as that of Ti^{4+} (0.68 Å) and Zr^{4+} (0.84 Å). Therefore, Cu^{2+} ions can substitute for Ti^{4+} or Zr^{4+} ions. Due to the charge difference, the system is compensated by the formation of oxygen vacancies (discussed in detail later). For diffusion-control mechanism in a sintering process, the most slowly diffusing species (often oxygen ions) should determine the overall rate of the reaction [161].

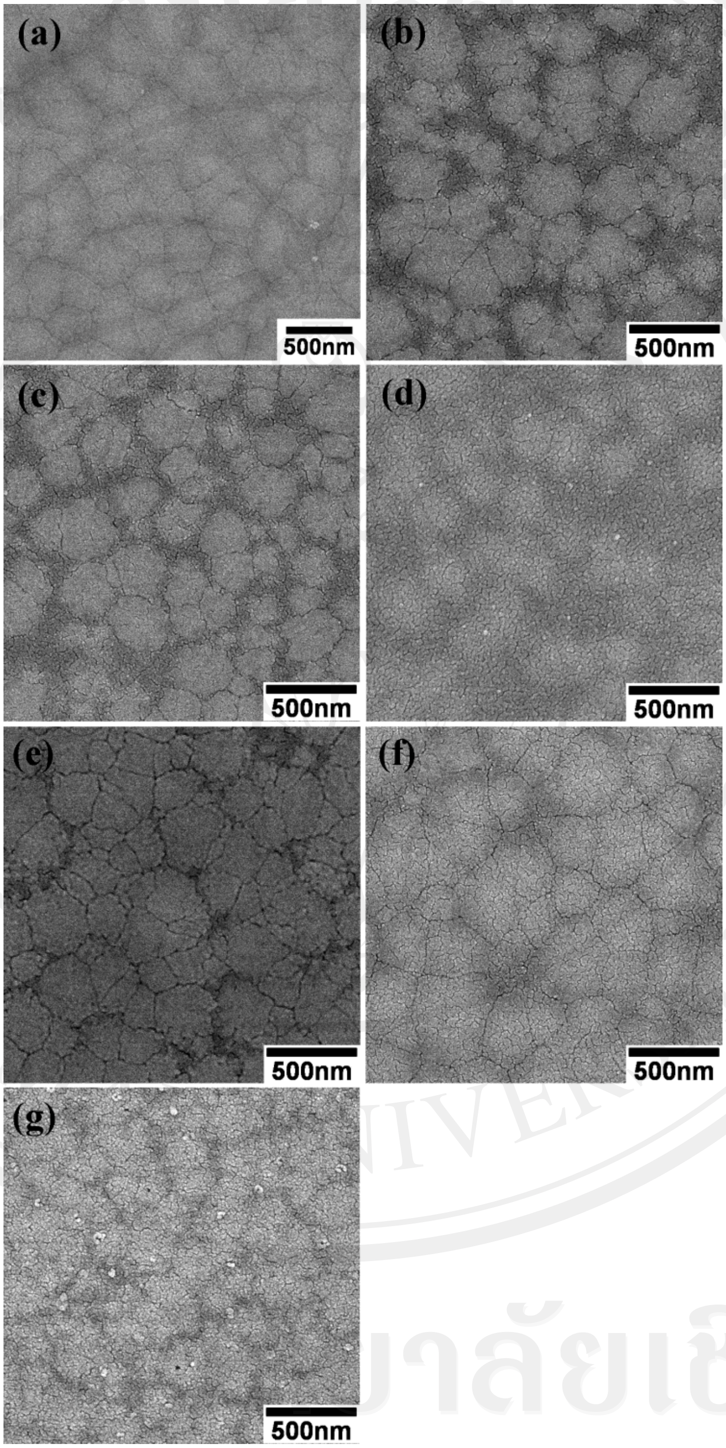

Figure 6.3 SEM micrographs of PZT/*x*CuO films' surfaces where *x* = (a) 0, (b) 0.1, (c) 0.2, (d) 0.3, (e) 0.4, (f) 0.5 and (g) 1 wt%, (magnification = × 40,000).

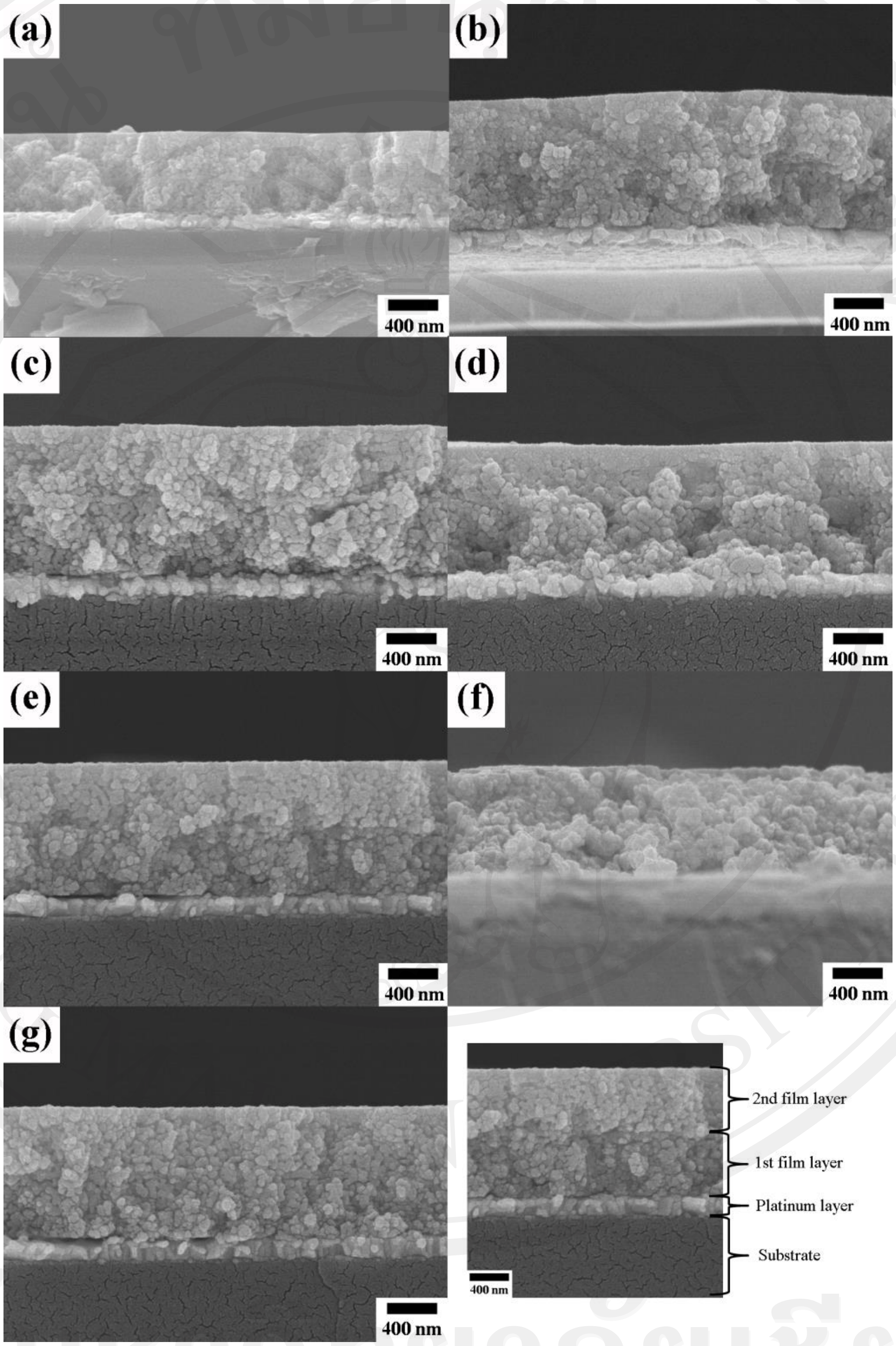

Figure 6.4 SEM micrographs of cross sections of PZT/*x*CuO films, where *x* = (a) 0, (b) 0.1, (c) 0.2, (d) 0.3, (e) 0.4, (f) 0.5 and (g) 1 wt%.

Thus, increasing the oxygen vacancy concentration would accelerate the sintering rate. However, with the CuO addition of 0.4 wt% and 1 wt%, the grain sizes slightly decreased. The reduction could be, as found in previous work [162], because of the formation of the Cu-rich second phase in the grain boundary where the particles of the second phase were insoluble. The insoluble particles decreased the grain boundary movement, and when the grain boundary tried to move past the inclusion, diffusion of atoms from one grain to another was hindered by the insoluble particles [163]. In this work, the second phase could be $Pb(Cu_2O_2)$ phase as shown in the XRD result in Fig. 6.2.

Table 6.1 Grain size and preferred orientation of PZT/*x*CuO films, where *x* = 0, 0.1, 0.2, 0.3, 0.4, 0.5 and 1wt%.

CuO (wt%)	Grain size (nm)	Peak intensity ratio (%)		
		(111)	(010)	(110)
0	56.99 ± 10.00	7	19	49
0.1	60.46 ± 09.10	7	18	53
0.2	72.93 ± 15.08	8	21	49
0.3	80.02 ± 23.25	7	21	49
0.4	73.18 ± 21.70	7	33	26
0.5	75.95 ± 20.00	6	37	23
1	76.05 ± 11.00	5	49	23

6.3 Electrical properties of PZT/CuO thin films

Electrical properties such as dielectric, ferroelectric and ferroelectric fatigue of PZT/*x*CuO, where *x* = 0, 0.1, 0.2, 0.3, 0.4, 0.5 and 1 wt%, were studied. Among these conditions, the best ferroelectric was selected, and the ferroelectric fatigue of acceptor doping compared to PZT thin film was studied.

6.3.1 Dielectric property of PZT/CuO thin films

Figure 6.5 shows dielectric constant (ε_r) and dielectric loss ($tan\delta$) of PZT/CuO films measured at room temperature plotted as a function of frequency (1-1000 kHz). Capacitance of the films as a function of frequency was measured by LCR meter at room temperature. Then, the dielectric constants were calculated by using equation 2.8.

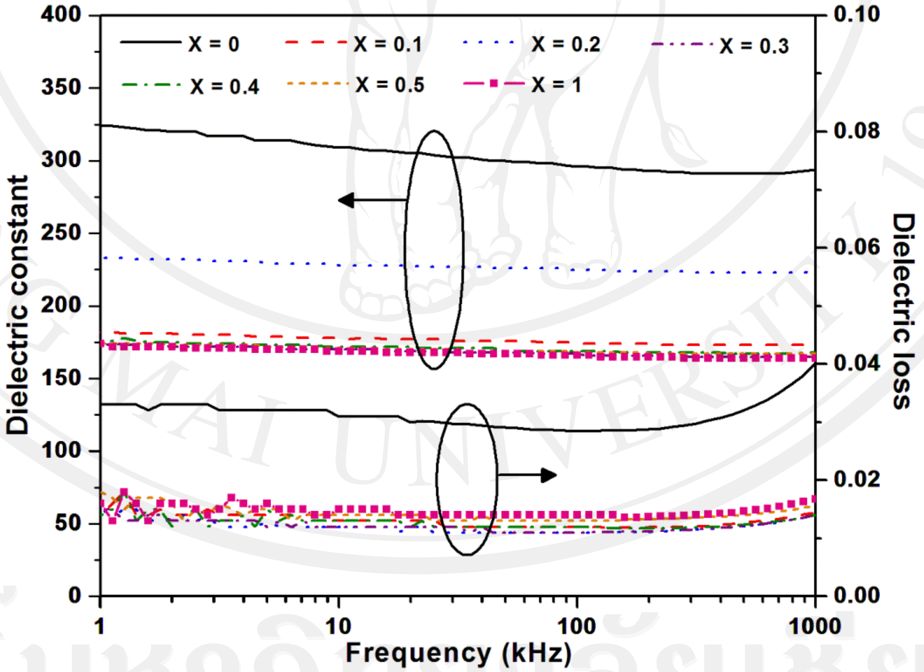

Figure 6.5 Frequency dependence of dielectric constant (ε_r) and dielectric loss ($tan\delta$) for PZT/xCuO films, where x = 0, 0.1, 0.2, 0.3, 0.4, 0.5 and 1 wt%.

The dielectric constant decreased with increasing frequency as described in the previous chapter while the dielectric loss showed less dependency on frequency. Regarding the PZT/CuO films, dielectric constant was reduced as CuO was added. Among the CuO-added PZT films, the film with 0.2 wt% CuO showed the maximum dielectric and ferroelectric properties, although the values were lower than those of pure PZT film as shown in Fig. 6.5. The dielectric constant and loss values at room temperature and at 1 kHz are also listed in Table 6.2. This phenomenon is described below.

6.3.2 Ferroelectric properties of PZT/CuO thin films

Polarization-electric field (*P*-*E*) hysteresis loops of PZT/*x*CuO films, where $x = 0$, 0.1, 0.2, 0.3, 0.4, 0.5 and 1 wt% at electric field 1000 kV/cm and a frequency of 1 kHz are presented in Fig. 6.6. The *P*-*E* hysteresis loops of PZT/CuO films showed a similar trend to that found in dielectric constant (Fig. 6.5). Except for PZT/0.2 wt% CuO, the polarization was reduced with increasing concentration of CuO. The data of dielectric and ferroelectric properties measured at room temperature are shown in Table 6.2. The reduction of dielectric and ferroelectric properties with increasing CuO concentration was explained by the substitution of CuO for PZT in which oxygen vacancies were expected to be created. The presence of the non-ferroelectric phase also contributed to the reduction and is described later. Furthermore, the increase of (010) preferential orientation with increasing CuO concentration caused polarization to be more difficult because the (010) orientation was perpendicular to spontaneous polarization of the rhombohedral phase [151]. The abrupt increase in polarization of PZT/0.2 wt% CuO film may be due partly to its homogeneous microstructure and a slightly higher fraction of (111) oriented grains as shown in Table 6.1. PZT (111) phases were previously reported to have good ferroelectric properties compared to other orientations [164]. The increase in coercive field (E_c) in PZT/CuO films may be explained by the increase in oxygen vacancies caused by acceptor doping effect on the B-site substitution of Cu^{2+} (r_{Cu2+} = 0.72 Å) for Ti^{4+} (r_{Ti4+} = 0.68 Å) or Zr^{4+} (r_{Zr4+} = 0.81) ions that were charge compensated by oxygen vacancies ($V_o^{\cdot\cdot}$) [156] as shown in equation (6.1). It was understood that the dopant oxide on the left side is substituted for the host (Zr, Ti)O_2 in PZT. Thus, the dopant oxide CuO, brought less oxygen per cation (O_o^x) into the PZT structure. The oxygen vacancies might be segregated to the domain walls and the electrode. This required a higher electric field for the domain wall motion, resulting in the higher E_c in CuO-added PZT films compared to that of pure PZT films (Fig. 6.7).

$$CuO \rightarrow Cu''_{Zr,Ti} + O_o^x + V_o^{\cdot\cdot} \qquad (6.1)$$

Moreover, the ferroelectric characteristics can be observed by the hysteresis loop squareness (R_{sq}) [148]. The squareness ratio of the hysteresis loop for ferroelectric materials, which is the ratios of the remanent polarization (P_r) at zero electric field to the maximum polarization (P_{max}) at the maximum applied field obtained at some finite field strength below the dielectric breakdown [149].

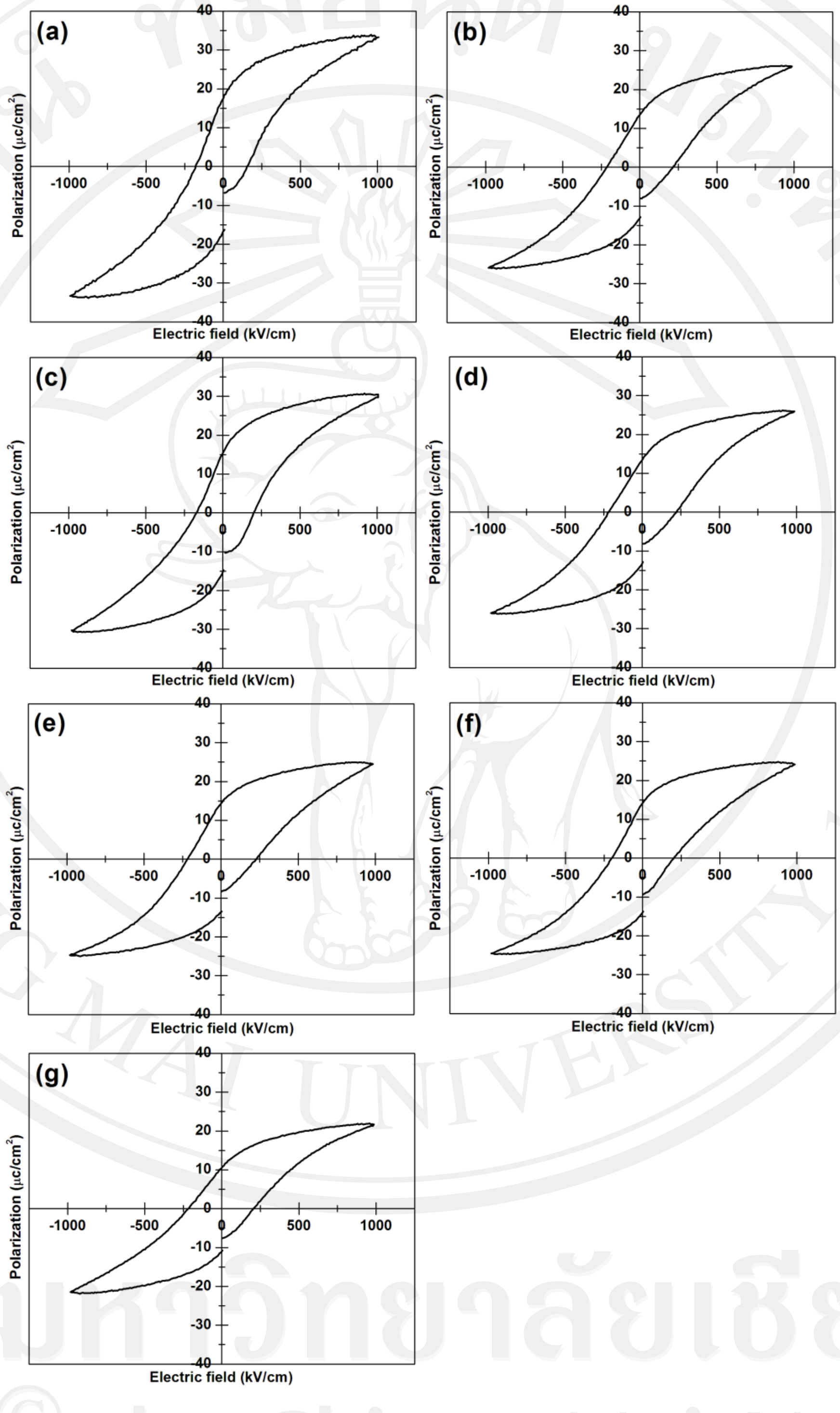

Figure 6.6 *P-E* hysteresis loops of PZT/xCuO films, where x = (a) 0, (b) 0.1, (c) 0.2, (d) 0.3, (e) 0.4, (f) 0.5 and (g) 1 wt%.

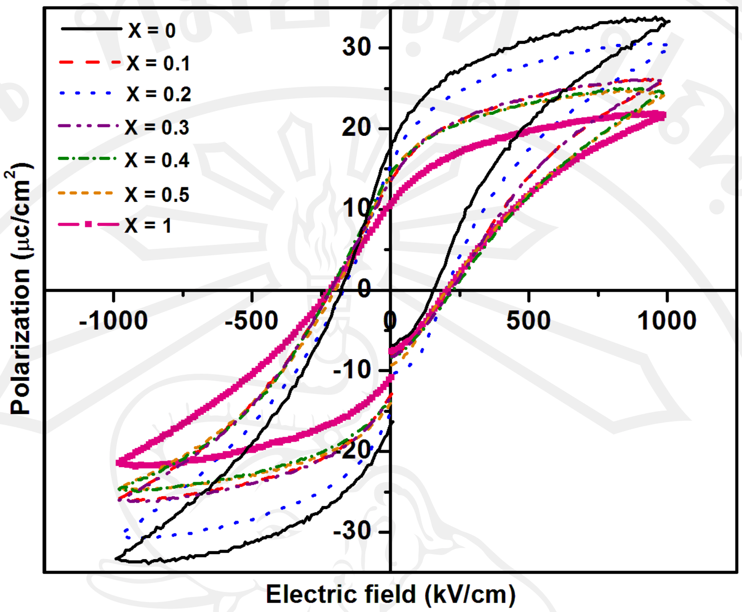

Figure 6.7 Comparison of *P-E* hysteresis loops of PZT/*x*CuO films, where *x* = 0, 0.1, 0.2, 0.3, 0.4, 0.5 and 1 wt%.

Table 6.2 Electrical properties of PZT/*x*CuO films, where *x* = 0, 0.1, 0.2, 0.3, 0.4, 0.5 and 1wt%.

CuO (wt%)	Electrical properties at room temperature					
	ε_r	$tan\delta$	P_{max}(μC/cm^2)	P_r(μC/cm^2)	E_c(kV/cm)	R_{sq}
0	324	0.033	33.68	17.63	175	0.61
0.1	182	0.014	26.14	13.69	220	0.62
0.2	233	0.015	30.71	15.68	217	0.73
0.3	174	0.014	26.18	13.24	221	0.60
0.4	176	0.018	24.94	14.57	227	0.66
0.5	174	0.016	24.73	14.36	209	0.67
1	174	0.015	21.91	10.79	207	0.58

Note: dielectric property was measured at 1 kHz; ferroelectric property was measured at 1 kHz and 1000 kV/cm applied field.

Squareness (calculated by equation 5.2) was used to measure not only the deviation in the polarization axis but also that in the electric field axis. The squareness of the films were calculated and showed in Table 6.2. It was found that the squareness of this system were not dependent on CuO concentration. Although squareness seemed to increase when CuO were added, the squareness of this system is in the range of 0.6 – 0.7, which was much lower compared to the ideal square loop of 2.0. This may occur as the loop did not get a saturated electric field due to the high saturation field of these PZT thin films and a limitation of equipment. The higher degree of loop squareness in PZT/CuO film than in PZT film showed the enhancement of ferroelectric interaction on PZT thin film. In addition, it is well known that the film for memory applications are required to possess the properties, such as a large remanent polarization (P_r), a low coercive field (E_c) and high degree of loop squareness (R_{sq}) [38, 45, 150]. In this system, the PZT/0.2 wt% CuO film showed the largest remanent polarization, the higher coercive field and the good loop squareness compare to the other compositions.

From the ferroelectric properties of PZT/CuO thin films, PZT/0.2wt%CuO thin films was found to be the best representative for acceptor doping (high coercive field due to the domain wall pinning by oxygen vacancies) compared to the other conditions in this system. Therefore, this work used PZT/0.2wt%CuO thin films to investigate the effect of acceptor doping on fatigue properties in PZT thin films.

6.3.3 Fatigue property of PZT/CuO thin films

Ferroelectric fatigue is a measurement of loss of switchable polarization (P_{sw}) with repeated polarization reversal [151]. Hysteresis loops of PZT film and PZT/CuO film before and after 10^8 polarization switching cycles were compared. The samples were electrically fatigued under an applied field of higher than about 3 times (about 500 kv/cm) of a switching electric field (E_{sw}) and at a fixed frequency at 1 kHz. Figures 6.8 (a-b) shows the fatigue behaviors of PZT and PZT/0.2 wt% CuO thin films plotted as a function of polarization switching cycles. For the PZT film, P_{sw} began to decrease after 10^6 cycles, and it was found to be reduced by 17% at 10^8 cycles. The switchable polarization of PZT/0.2 wt% CuO increased at 10^4 cycles and then began to decrease after 10^5 cycles. Ultimately, it was reduced by 14% at 10^8 cycles. The increase in switchable polarization at 10^4 cycles was possibly due to as-deposited polycrystalline films are generated a random orientation (Fig. 6.4) particularly in doping samples. This led to a reduction in the maximum possible total polarization (described in detail in the next chapter). Nevertheless, the reduction of switchable polarization appeared earlier than that in PZT film. A possible mechanism for this phenomenon was that Cu^{2+} occupied the B-site (Ti^{4+} and Zr^{4+}) in PZT [157], resulting in the compensation of the charge difference by oxygen vacancies as shown in equation 6.1. This was responsible for the reduction of switchable polarization in PZT/0.2 wt% CuO thin film. However, 14% reduction of switchable polarization at 10^8 cycles was less than 17% at 10^8 cycles in PZT thin film. It was demonstrated that hard PZT film was more stable under a continuous cyclical drive compared to pure PZT film due to their inherent polarization pinning effect and good electrical strength [165].

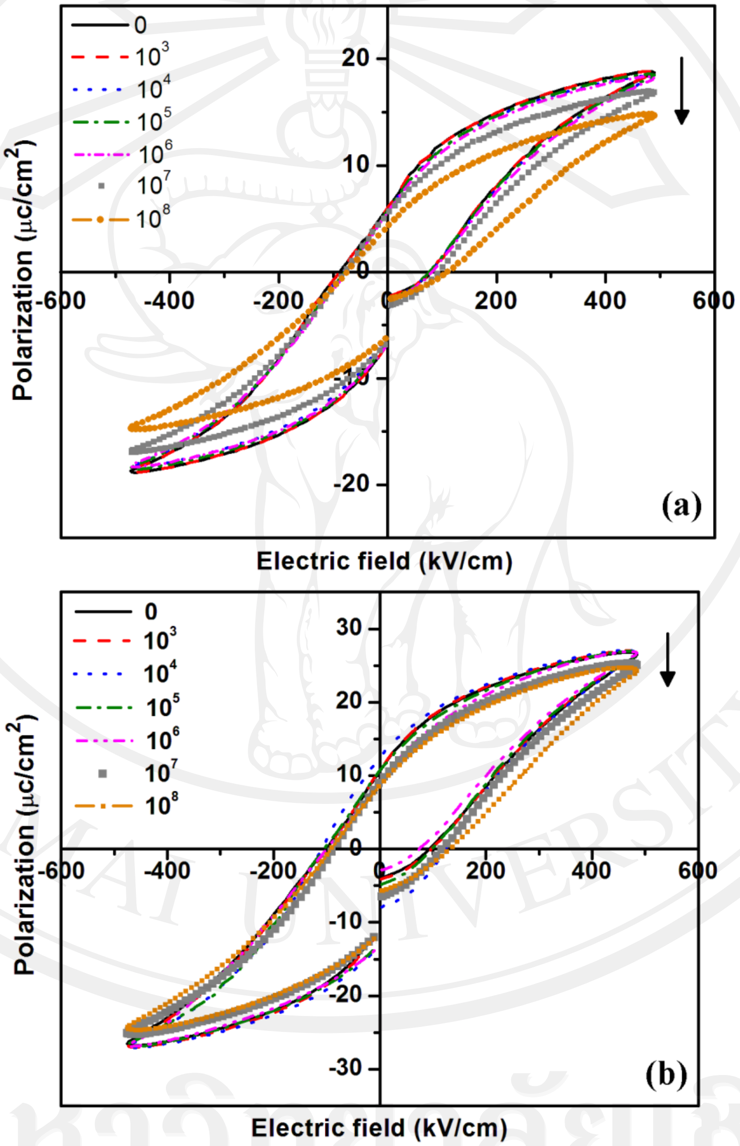

Figure 6.8 Hysteresis loops of (a) PZT and (b) PZT/0.2 wt% CuO films plotted at different bipolar fatigue cycles under 500 kV/cm at 1 kHz.

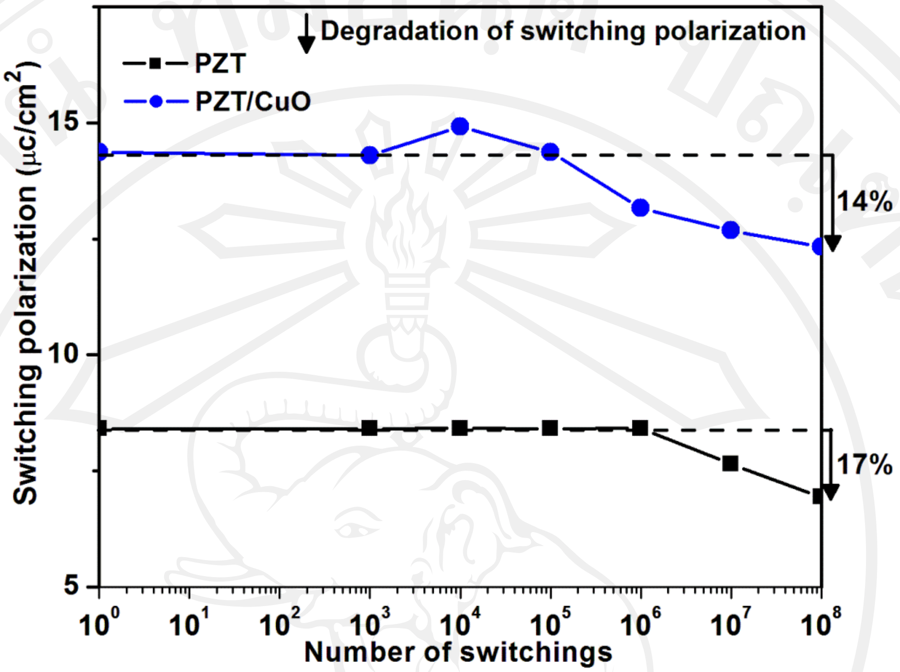

Figure 6.9 Switchable polarization of PZT and PZT/CuO thin films plotted as a function of bipolar fatigue cycles.

6.4 Conclusions

The effects of CuO nanoparticles on phase and electrical properties of PZT thin films were investigated. The PZT/xCuO films (where x = 0, 0.1, 0.2, 0.3, 0.4, 0.5 and 1 wt%) were prepared by a hybrid chemical solution deposition technique. It was found that 600°C was sufficient for film annealing in order to obtain a complete perovskite phase. In addition, the reaction of PbO and CuO forming $Pb(Cu_2O_2)$ was observed in a relatively high concentration of CuO (≥ 0.4wt%). The changes of preferred orientation of PZT/CuO films depended upon CuO concentration. The microstructures of films were dense for all the films, indicating that the CuO-added PZT films promoted the grain growth of PZT films. The dielectric and ferroelectric properties of PZT films reduced with increasing coercive field (E_c) when CuO were added. Among the CuO added PZT films, the PZT film with 0.2 wt% CuO concentration showed the maximum dielectric and ferroelectric properties possibly due to the influence of microstructural homogeneity and higher fraction of high polarizability (111) oriented grains. Because of the increase of E_c, adding CuO resulted in an acceptor-doped PZT film with the role of oxygen vacancies inducing hard ferroelectric behavior in these PZT/CuO films. Improved fatigue behavior was also observed in this PZT/CuO system because of its inherent polarization pinning effect and good electrical strength. Compared to the 17% reduction of polarization found in PZT films at 10^8 cycles, the improvement in PZT fatigue behavior was obtained when 1 wt% of WO_3 was added into PZT thin films, resulting in the 14% reduction of switchable polarization up to 10^8 switching bipolar pulses.